Processing and Application of Ceramics 11 [3] (2017) 177–184
https://doi.org/10.2298/PAC1703177K

Structural and optical characterizations of $BaSnO_3$ nanopowder synthesized by aqueous sol-gel method

Upendra Kumar, Md. Jawed Ansaree, Shail Upadhyay*

Department of Physics, Indian Institute of Technology (Banaras Hindu University), Varanasi - 221005, U.P., India

Received 12 November 2016; Received in revised form 31 January 2017; Received in revised form 23 June 2017; Accepted 10 August 2017

Abstract

Precursor gel for preparation of nanocrystalline $BaSnO_3$ powder was synthesised by aqueous sol-gel method using $Ba(OH)_2 \cdot 8\,H_2O$ and $Na_2SnO_3 \cdot 3\,H_2O$ as raw materials. Thermogravimetric and differential scanning calorimetric analyses of the raw materials, precursor gel and a mechanical mixture of raw materials were carried out to understand the mechanisms involved in the formation of the single phase $BaSnO_3$. Based on the thermal analysis, the precursor gel was calcined at 400, 800 and 1400 °C for 4 h to obtain pure phase $BaSnO_3$ powder. X-ray diffraction pattern of the powder calcined at 1400 °C was refined for atomic coordinate, lattice parameter (a = 4.1117(2) Å) and occupancies using Rietveld refinement analysis. The average crystallite size calculated from the Scherrer formula is ~35 nm. Transmission electron micrograph of the powders confirmed that particle sizes are in range of 20–40 nm. The phase purity of the powder calcined at 1400 °C was further examined by Fourier transform infrared spectroscopy. Optical properties of the $BaSnO_3$ powder were studied by UV-visible absorption and photoluminescence (PL) spectra. The band gap energy (3.09 eV) obtained from the Tauc plot confirmed the semiconductor nature of the powder. The CIE coordinate corresponding to PL spectrum exhibited an intense emission in the visible region.

Keywords: *$BaSnO_3$, sol-gel, structural characterization, optical properties*

I. Introduction

In the last decade, $BaSnO_3$ has drawn attention due to its properties, such as n-type semiconductivity [1], high electrical conductivity and optical transparency in visible region [2–4]. $BaSnO_3$ has been used as solid state gas sensor [5,6], an electrode material for the dye-sensitized solar cell [7], anode material for lithium-ion battery [8], photocatalyst [9] and proton conductor for fuel cell [10]. The various methods were used to prepare barium stannate such as: high temperature solid state [11], sol-gel combustion [12,13], hydrothermal [14], polymeric precursor [15], lyothermal [16], wet chemical [17], chemical precipitation [18] and reverse micelles method [19]. Among the reported chemical methods, an aqueous sol-gel method is found to be a simple, cost-effective and low-temperature chemical method for the synthesis of $BaSnO_3$. For the same preparative method, the selection of reactants for the formation of $BaSnO_3$ plays a crucial role in quality control and hence properties of the powder. Efforts have been made to synthesize $BaSnO_3$ nanopowder at a lower temperature by using different Ba and Sn compounds [20]. Huang *et al.* [21] tried to use lower temperature by ball-milling a mixture of $BaCO_3$-SnO_2 for prolonged period of 40 h in an air atmosphere and showed that the formation of $BaSnO_3$ was initiated at temperature 820 °C. Cerda *et al.* [12] synthesized $BaSnO_3$ at 1100 °C by an aqueous sol-gel method using $Ba(OH)_2$ and K_2SnO_3. The used method seems to be a simple and cost-effective in terms of less number of steps involved in the preparation, but in this report details about the mechanism of the formation of $BaSnO_3$ powder have not been discussed. Therefore, in the present work, an attempt has been made to understand each and every step involved in the formation of phase pure nanocrystalline $BaSnO_3$ powder by an aqueous sol-gel method using $Ba(OH)_2$ and Na_2SnO_3 as raw

* Corresponding author: tel: +91 542 6702006,
fax: +91 542 2368428, e-mail: *supadhyay.app@itbhu.ac.in*

materials. The intension behind using Na_2SnO_3 in place of K_2SnO_3 used by earlier authors is that sodium is more reactive than potassium and hence it could more easily react with water and form NaOH which will accelerate reaction rate. Simultaneous thermogravimetric (TG) and differential scanning calorimetric (DSC) analysis and XRD techniques were used to understand the formation mechanism of $BaSnO_3$ nanocrystals. Structural and optical characterizations of the obtained phase pure $BaSnO_3$ powder were performed with different techniques.

II. Experimental

2.1. Powder synthesis

The stoichiometric amounts of raw materials, $Na_2SnO_3 \cdot 3\,H_2O$ (99% purity, Molychem) and $Ba(OH)_2 \cdot 8\,H_2O$ (98% purity, Molychem), were dissolved separately in minimum quantities of distilled water. The solutions of barium hydroxide and sodium stannate were mixed homogeneously using a magnetic stirrer maintained at a constant rotation speed of 200 rpm for 3 h at 80 °C. pH of the solution was measured several times using a digital pH meter and found to be ~11. Thereafter, the solution was heated on a hot plate at 150 °C for several hours until formation of gel took place. The precursor gel was calcined at 400, 800 and 1400 °C for 4 h.

2.2. Powder characterization

Thermal analysis of the raw materials, precursor gel and mechanical mixture of raw materials were carried out in the temperature range 25–1000 °C in a simultaneous TG/DSC setup (Mettler Toledo) with a heating rate 10 °C/min in a nitrogen gas atmosphere. Phase identification and structural characterization of the obtained powders were carried out using a Rigaku Mini Flex-II desktop X-ray diffractometer, with Ni-filtered Cu-Kα (1.5405 Å) radiation at 30 kV and 20 mA. XRD patterns of the calcined powder were recorded over the angular range $20° \leq \theta \leq 80°$ with step size 0.02° (2θ). Transmission electron micrographs (TEM) of the obtained powders were recorded using FEI Tecnai Model G2 series. The specimen was prepared by dispersing the powder in ethyl alcohol by ultra-sonication for 1 h. Thereafter, the solution was poured on a commercial carbon-coated copper grid and dried in a petri dish at 60 °C for 2 h in a hot air oven. Fourier transform infrared (FTIR) spectrum of the samples was recorded using Fourier transform infrared spectrometer (Shimadzu, Model DF 803) using KBr pellet method in the wave number range 400–4000 cm^{-1}. The UV-visible spectrum of the synthesized $BaSnO_3$ nanopowder was recorded (Shimandzu, model UV-1700) using ethylene glycol as a suspension medium. The photoluminescence spectroscopy (PL) of the nanopowder was performed using Horiba photometry with Xe lamp as a source.

III. Results and discussion

3.1. Thermal analysis

Figure 1a shows TGA-DSC curves of the raw material $Ba(OH)_2 \cdot 8\,H_2O$. TGA curve exhibits total weight loss of ~48% within the measured temperature range of 25–1000 °C in three steps. The first step weight loss (42.88%) in the temperature range of 30–150 °C accompanied by an endothermic peak around 90 °C is attributed to expulsion of physically absorbed water molecules according to the reaction (1):

$$Ba(OH)_2 \cdot 8\,H_2O \longrightarrow Ba(OH)_2 + 8\,H_2O \qquad (1)$$

However, the experimentally observed weight loss (42.88%) is slightly lower than the theoretical weight loss (~45%) calculated according to the reaction (1). This indicates that complete expulsion of water molecules (8 moles) is not taking place, may be due to the fast heating rate (10 °C/min) used during TGA data collection. The second step weight loss (~2%) accompanied by an endothermic peak around 384 °C is associated with removal of remaining water molecules. TGA curve of $Ba(OH)_2 \cdot 8\,H_2O$ observed in this work is in agreement with the TGA curve reported in the literature for this hydroxide [22]. The third step weight loss

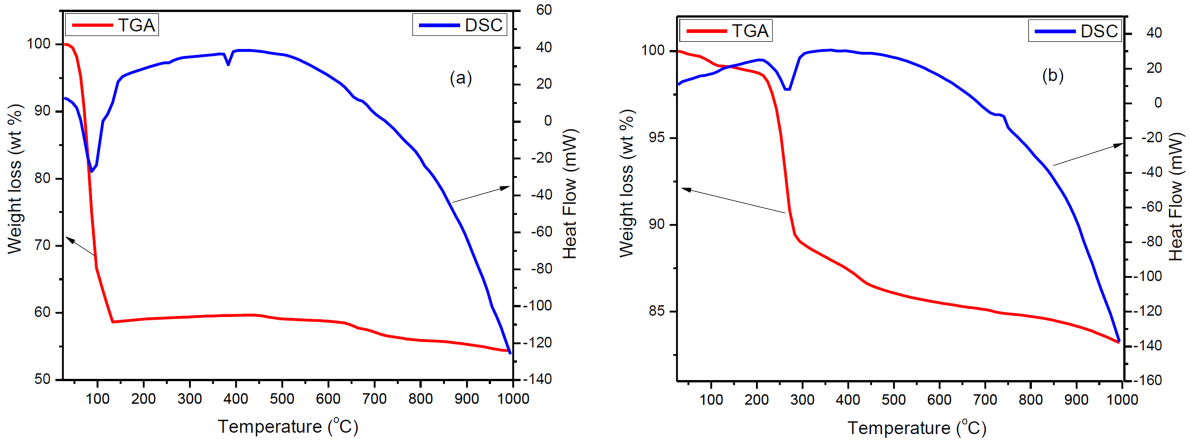

Figure 1. The simultaneous TGA-DSC curves of starting materials: a) $Ba(OH)_2 \cdot 8\,H_2O$ and b) $Na_2SnO_3 \cdot 3\,H_2O$

(3.12%) in the temperature of 600–700 °C corresponds to the loss of water molecules produced during conversion of $Ba(OH)_2$ into BaO described with reaction (2):

$$Ba(OH)_2 \longrightarrow BaO + H_2O \quad (2)$$

TGA-DSC curves of $Na_2SnO_3 \cdot 3\,H_2O$ are shown in Fig. 1b. Total weight loss of 17.05% has been observed in the entire range of temperature measurement. The observed experimental weight loss is less than the theoretical weight loss (20%) calculated according to equation (3):

$$Na_2SnO_3 \cdot 3\,H_2O \longrightarrow Na_2SnO_3 + 3\,H_2O \quad (3)$$

The weight loss of 17.05% occurs in two steps. The first step of weight loss (11.22%) was observed in the temperature range 27–300 °C and is assigned to the expulsion of water molecule according to reaction (4):

$$Na_2SnO_3 \cdot 3\,H_2O \longrightarrow Na_2SnO_3 \cdot H_2O + 2\,H_2O \quad (4)$$

In the literature, it is reported that dissociation of anhydrous Na_2SnO_3 into Na_2O and SnO_2 occurs at 900 °C. In our case Na_2SnO_3 is in hydrated form, therefore, dissociation may take place at a temperature lower than 900 °C. Accordingly, the second step weight loss (6.05%) observed in the temperature range 300–1000 °C is accompanied by an exothermic peak around 750 °C assigned to the dissociation of hydrated sodium stannate into sodium and tin oxides and gradual loss of chemically adsorbed water molecule according to reaction (5):

$$Na_2SnO_3 \cdot H_2O \longrightarrow Na_2O + SnO_2 + H_2O \quad (5)$$

The result obtained from the TGA-DSC analysis of $Na_2SnO_3 \cdot 3\,H_2O$ is in agreement with earlier reports [23].

A stoichiometric mixture of the raw materials $Ba(OH)_2 \cdot 8\,H_2O$ and $Na_2SnO_3 \cdot 3\,H_2O$ for the formation of $BaSnO_3$ by solid state ceramic route was prepared by their mechanical mixing in an agate mortar for 1 h using acetone as mixing media. The TGA-DSC curves of the obtained mixture were shown in Fig. 2a. The curves display combined features of both components as shown in Fig. 1, i.e. $Ba(OH)_2$ converts into BaO (above 700 °C) and Na_2SnO_3 into Na_2O and SnO_2 (above 750 °C). In the measured temperature range, BaO, Na_2O, and SnO_2 oxides are retaining their individuality, and no chemical reaction between them is taking place to form $BaSnO_3$ phase or any other phase up to 1000 °C. In other words, the formation of $BaSnO_3$ by solid state ceramic route using $Ba(OH)_2 \cdot 8\,H_2O$ and $Na_2SnO_3 \cdot 3\,H_2O$ may not take place before 1000 °C. In this work, the thermal analysis of a physical mixture of $Ba(OH)_2 \cdot 8\,H_2O$ and $Na_2SnO_3 \cdot 3\,H_2O$ was carried out just to show if the formation of $BaSnO_3$ is possible by solid state route or not. In order to understand the mechanism of the formation of $BaSnO_3$ using $Ba(OH)_2 \cdot 8\,H_2O$ and $Na_2SnO_3 \cdot 3\,H_2O$ in a solid form more studies are required.

In the present work $BaSnO_3$ powder was synthesised using $Ba(OH)_2 \cdot 8\,H_2O$ and $Na_2SnO_3 \cdot 3\,H_2O$ by an aqueous sol-gel method and formation mechanism of $BaSnO_3$ has been studied in detail. The TGA-DSC curves of the dried precursor gel powder are shown in Fig. 2b. It is noticed that TGA-DSC curves of the precursor gel powder are entirely different from the TGA-DSC curves of a mechanical mixture of starting materials (Fig. 2a). TGA curve of the precursor gel shows total weight loss (2%) in three steps. The first step weight loss between 25–150 °C (0.22%) may be due to the dehydration of water, the second step weight loss (0.48%) in the temperature range of 600–720 °C is attributed to the decomposition of $BaCO_3$. The third weight loss (1.30%) is accompanied by a small endothermic peak (at 800 °C) and attributed to the reaction between $BaCO_3$ and SnO_2 to form $BaSnO_3$. Weight loss of only 1.3% in the third step indicates that precursor gel powder already contains more than 90% of $BaSnO_3$ phase. Remaining 10% of gel powder contains impurity phases $BaCO_3$ and SnO_2. These impurity phases react with each other to form $BaSnO_3$ phase around 800 °C, which is evident from a small endothermic peak in DSC curve. Therefore, it is clear that formation of $BaSnO_3$ using $Ba(OH)_2 \cdot 8\,H_2O$ and $Na_2SnO_3 \cdot 3\,H_2O$ by an aque-

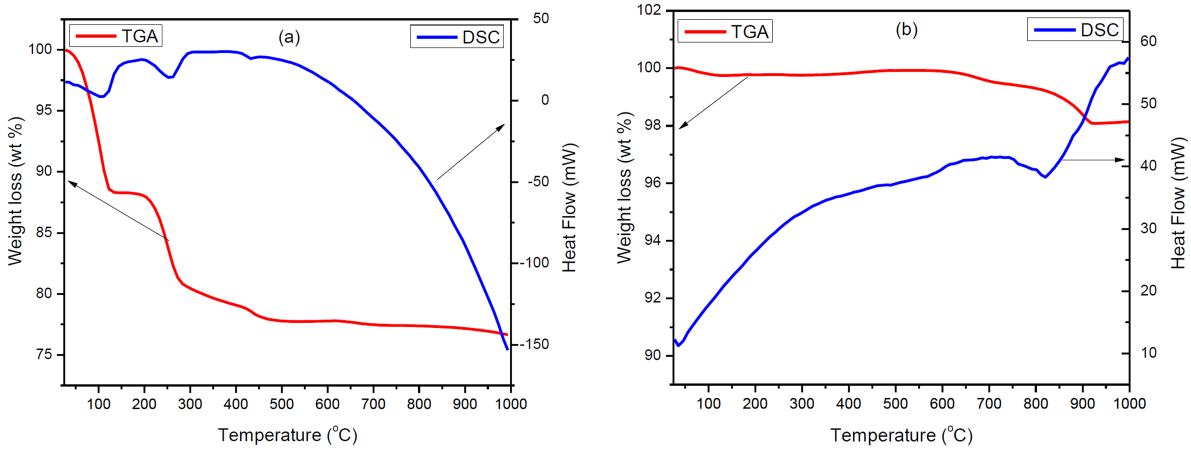

Figure 2. The simultaneous TGA-DSC curves of: a) mechanical mixture of raw materials and b) precursor powder gel

ous sol-gel method takes place at a lower temperature than solid state ceramic route. Based on the TGA-DSC results of precursor gel it is assumed that starting from the solution up to the formation of the gel, following possible reactions could take place:

$$Ba(OH)_2 \cdot 8\,H_2O + H_2O \longrightarrow Ba^{2+} + 2\,[OH]^- \quad (6)$$

$$Na_2SnO_3 + 3\,H_2O \longrightarrow 2\,Na^+ + [Sn(OH)_6]^{2-} \quad (7)$$

$$[Sn(OH)_6]^{2-} + Ba^{2+} \longrightarrow BaSn(OH)_6 \quad (8)$$

$$2\,Na^+ + 2\,OH^- \longrightarrow 2\,NaOH \quad (9)$$

$$BaSn(OH)_6 \longrightarrow BaSnO_3 + 3\,H_2O \quad (10)$$

Ba^{2+} ions react very easy with CO_2. Therefore, those Ba^{2+} ions which are present on the surface of the solution may react with the CO_2 present in the atmosphere to form $BaCO_3$ phase. Similarly, Sn^{4+} ions may also react with the O_2 present in the ambient atmosphere and form SnO_2 phase.

3.2. XRD analyses

X-ray diffraction patterns of the precursor gel and the powders obtained after calcination of the precursor gel powder at 400, 800 and 1400 °C for 4 h are shown in Fig. 3. It can be noticed that XRD patterns of the precursor gel and powder calcined at 400 °C are similar and mainly amorphous in nature with some diffraction peaks of $BaCO_3$ and SnO_2 phases, which are well matched to the JCPDS file no 05-0378 and 41-1445, respectively. Therefore, the formation of $BaCO_3$ and SnO_2 phases have taken place by reaction of Ba^{2+}/Sn^{4+} ions (from $Ba(OH)_2 \cdot 8\,H_2O$ and $Na_2SnO_3 \cdot 3\,H_2O$) present in the water solutions with CO_2/O_2 gasses present in the atmosphere as discussed in TGA-DSC section.

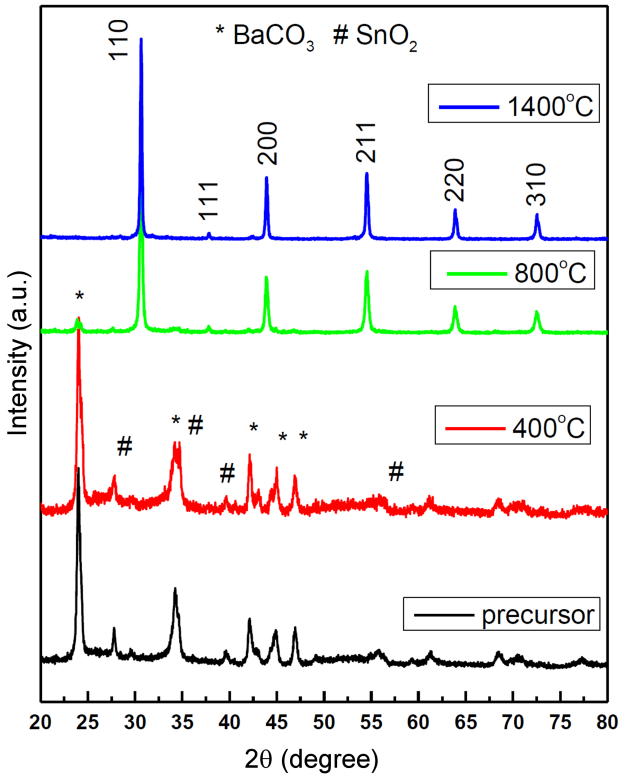

Figure 3. X-ray diffraction pattern $BaSnO_3$ of powder calcined at different temperatures

XRD pattern of the powder calcined at 800 °C contains mainly diffraction peaks of $BaSnO_3$ phase (JCPDS file no. 15-0780) except for a weak XRD peak (~23.8°) of $BaCO_3$ phase. It was reported in the literature [24] that formation of $BaSnO_3$ using commercially available $BaCO_3$ and SnO_2 by conventional solid state ceramic method requires temperature ≥1000 °C. In this work, the thermal analysis of a mechanical mixture of $Ba(OH)_2 \cdot 8\,H_2O$ and $Na_2SnO_3 \cdot 3\,H_2O$ also confirmed that formation of $BaSnO_3$ by solid state ceramic route will take place at temperatures >1000 °C. In XRD pattern of the powder calcined at 1400 °C only peaks of $BaSnO_3$ phase are present which shows that the powder obtained at this temperature is devoid of any impurity phase. Reitveld refinement of the XRD data of the powder calcined at 1400 °C was performed using software Full Proof and it is shown in Fig. 4. Based on the Rietveld analysis the structure of the synthesized $BaSnO_3$ powder was found to be cubic perovskite structure with space group *Pm3m* and its crystal structure is shown as the inset in Fig. 4. The lattice parameters obtained by the Rietveld refinement (a = 4.11172 ± 0.0015 Å, unit cell volume V = 69.38 Å^3 and theoretical density ρ = 7.277 g/cm^3) are in good agreement with the values re-

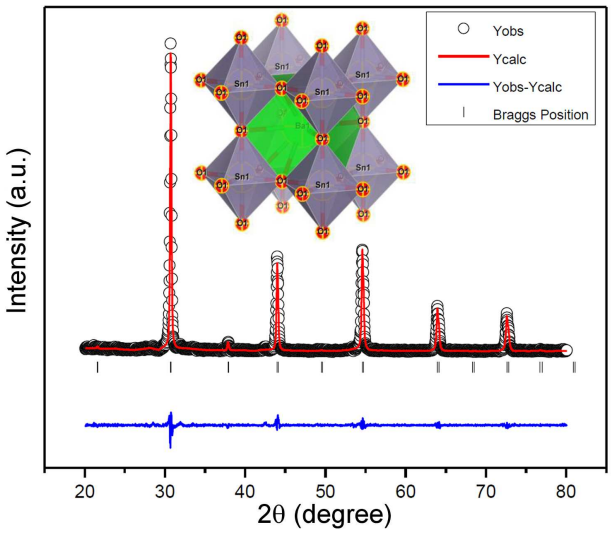

Figure 4. X-ray Rietveld refinement of $BaSnO_3$ powder calcined at 1400 °C (Yobs, Ycal, Yobs-Ycal and Bragg's positions represent the experimental data, calculated data, the difference between the two and Bragg's positions, respectively)

Table 1. Atomic coordinates and occupancies of elements of $BaSnO_3$

Atom	Site	x	y	Z	B	Occ.
Sn	1a	0	0	0	1.02	1
Ba	1b	0.5	0.5	0.5	0.89	1
O	3d	0.5	0	0	0.56	3

Table 2. Plane, diffraction angle (2θ), full width at half maximum (β) and crystallite size (D) of powders obtained after heat treatment at 800 °C and 1400 °C

No.	Plane	2θ [°]	Powder calcined at 800 °C		Powder calcined at 1400 °C	
			β [°]	D [nm]	β [°]	D [nm]
1	(110)	30.62	0.2833	29.08	0.2099	39.20
2	(111)	37.82	0.3048	30.92	0.2166	38.80
3	(200)	44.92	0.1466	37.31	0.2521	34.00
4	(211)	54.44	0.3277	27.27	0.2942	30.40
5	(220)	63.85	0.4196	22.31	0.3427	28.35
6	(310)	72.41	0.4477	22.00	0.3955	33.45
			Average size is 28.14		**Average size is 34.80**	

ported in the literature [25]. Atomic coordinates and occupancies are given in Table 1. The fitting parameters obtained after the refinement are $\chi^2 = 5.90$, $R_p = 8.8\%$, $R_{wp} = 8.18$.

The crystallite sizes D were calculated using Scherrer's formula:

$$D = \frac{0.9\lambda}{\beta \cdot \cos\theta_{max}} \tag{11}$$

where λ is wavelength of X-rays, β is the full width at half maximum of the particular ($h\ k\ l$) plane in radians and θ_{max} is the corresponding incident angle. The value of crystallite size of powders obtained after calcination at 800 °C and 1400 °C are given in Table 2. The average crystallite size of the powders obtained after calcination at 800 and 1400 °C is ~28 nm and 35 nm, respectively.

3.3. Transmission electron microscopy analyses

Transmission electron micrograph (TEM) of the precursor gel calcined at temperature 1400 °C for 4 h is shown in Fig. 5a. According to the TEM results it is clear that particles have sizes in the range from 10 to 40 nm and cubic shape similar to their unit cell. Histogram of the particle size distribution, obtained using software ImageJ, is shown in Fig. 5b. From the particle size distribution fitted by Gaussian function the average grain size was calculated to be 25 nm, which is slightly lower than the crystallite size ~35 nm (Table 1) calculated using Scherrer's formula. Selected area electron diffraction (SAED) pattern of the powder, presented in Fig. 5c, shows sparser ring pattern typically exhibited by poly-crystalline materials [26]. It is verified that diffraction spots present in the SEAD pattern belong to $BaSnO_3$. The Miller indices ($h\ k\ l$) of diffracting planes were calculated using values of inter planar spacing, d, obtained from the pattern. These values are 1.475, 1.861, 2.359 and 1.646 Å and corresponding Miller indices of planes are (220), (102), (111) and (112). The average value of the lattice parameter calculated using SAED is 4.11204 Å which is consistent with value (4.11172 Å) obtained from the Rietveld refinement of X-ray diffraction data.

3.4. Fourier transform infrared spectroscopy

Fourier transform infrared (FTIR) spectra of the synthesized powders were recorded to check the presence of $BaCO_3$, the most commonly found impurity phase detected in the preparation of $BaSnO_3$. According to the reported literature [27], FTIR was found to be the most sensitive technique for the detection of $BaCO_3$ (down to 0.6%). FTIR spectra of the $BaSnO_3$ powders calcined at 800 and 1400 °C are shown in Fig. 6. The distinct feature of the FTIR spectra is a band around 640 cm^{-1} characteristic for stretching mode of Sn–O bonds [28]. The presence of this band confirms the formation of $BaSnO_3$ phase. The width of this band is particle size dependent. Therefore, the width of the band is broad for the powder calcined at 1400 °C as compared to the powder calcined at 800 °C. Moreover, FTIR spectrum of the powder calcined at 800 °C has a few more bands. The weak absorption bands around 850, 1050 and 1430 cm^{-1}

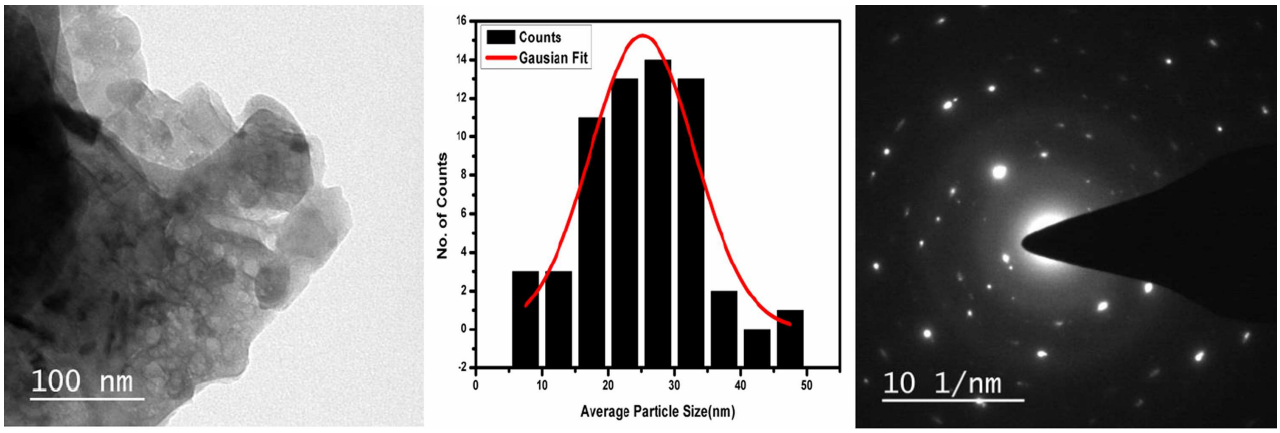

Figure 5. TEM image (a), Gaussian distribution plot (b) and selected area electron diffraction pattern (c) of prepared $BaSnO_3$ sample calcined at temperature 1400 °C

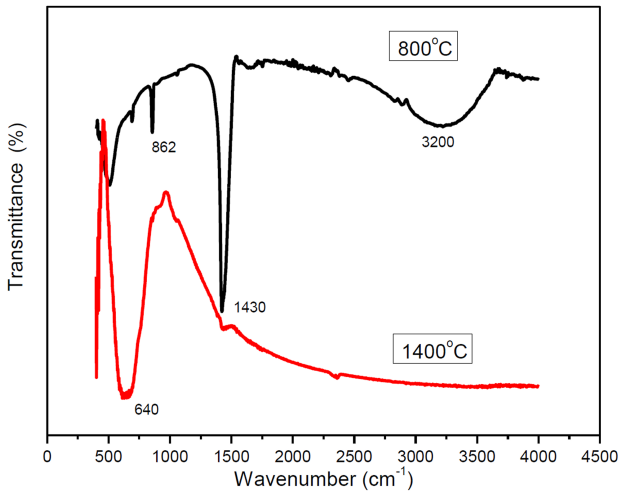

Figure 6. FTIR spectra of $BaSnO_3$ powder calcined at two different temperatures

in the FTIR spectrum of the powder calcined at 800 °C indicate the presence of impurity $BaCO_3$ phase [29]. In the FTIR spectra of the powder at 800 °C there is also a wide band of –OH group observed at 3200 cm^{-1}. On the other hand, all observed bands in the spectrum of the powder calcined at 1400 °C match with bands present in the FTIR spectrum of the pure phase $BaSnO_3$ reported in the literature [30].

3.5. *UV-visible spectroscopy*

The absorption spectrum of the powder calcined at 1400 °C was recorded in the wavelength range 200–800 nm by dispersing powder in ethylene glycol and it is shown in Fig. 7a. The absorption spectrum of $BaSnO_3$ powder synthesized in this work is similar to the spectrum exhibited by wide band gap semiconductor oxide [31]. The spectrum shows an absorption band around 445 nm which is due to the electron transfer from the top of the valance band to the bottom of the conduction band [32]. The band gap energy is the energy difference between the highest occupied molecular orbital (HOMO) to the lowest unoccupied molecular orbital (LUMO) and is termed as E_g. A better estimation of the band gap energy (E_g) was also obtained using Tauc's relation. According to this relation, the absorption coefficient for a direct band gap material is given by:

$$\alpha \cdot h \cdot \nu = B \cdot \left(h \cdot \nu - E_g\right)^m \tag{12}$$

where B is a constant independent of energy, E_g optical band gap energy, h is Planck's constant, ν is frequency of the incident photon and m is an index which depends on the nature of electronic transition responsible for the optical transition (m = ½ for direct transition and m = 2 for non-direct transition). Tauc's plot (using data shown in Fig. 7a) for band gap energy calculation was generated and shown in Fig. 7b. The direct energy band gap can be obtained from the intercept of the resulting linear region with the energy axis at $(\alpha \cdot h \cdot \nu)^2 = 0$. The band gap was calculated and found to be 3.09 eV, which is in agreement with value reported in the literature [31,32]. Slight difference in the value of energy band gap obtained from Fig. 7 may be due to the quantum size effect described by Koferstein and Yakuphanoglu [33], i.e. as the particle size of the system decreases the gap between the conduction band and the valance band also known as band gap of the material increases.

3.6. *Photoluminescence (PL) spectroscopy*

The photoluminescence spectrum (PL) of the powder calcined at 1400 °C (Fig. 8a) was recorded by exciting the powder using a source with the wavelength of 380 nm. The transitions between energy levels of constituent elements barium (Ba) and tin (Sn) of the compound $BaSnO_3$ cause emissions. The emission peaks exhibited by the synthesized powder are identified using data prepared by Sansonetti and Martin [34] and given in Table 3. This result indicates that the material has luminescence properties and it gives the intense emission in the visible region due to the transfer of charge between Sn^{2+}–O^{2-} levels [35]. Besides this strong intensity emission, spectrum also exhibits few emissions of weak intensity. The weak intensity emissions may

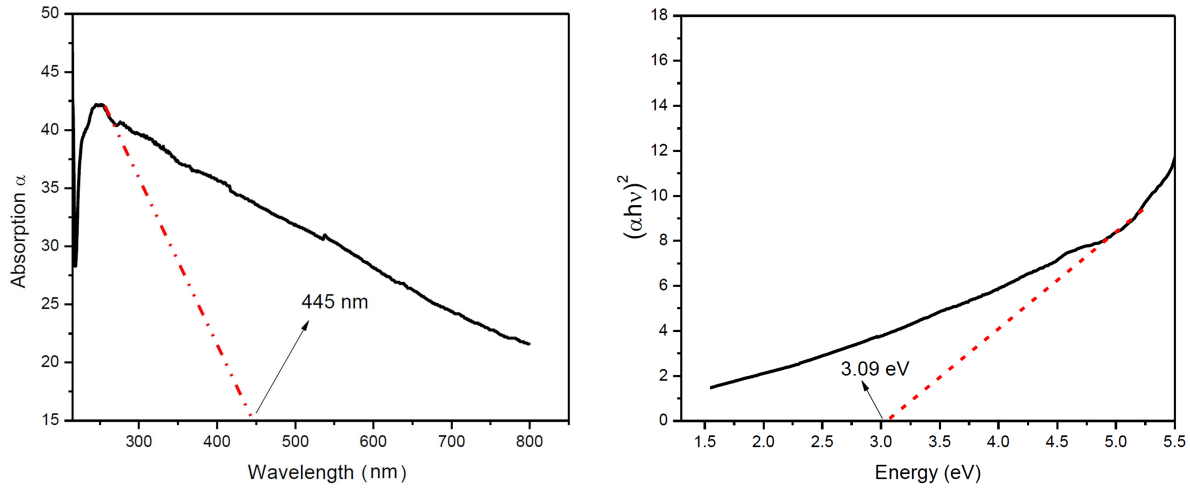

Figure 7. Absorption spectra of $BaSnO_3$ powder (a) and plot of $(\alpha \cdot h \cdot \nu)^2$ vs. photon energy (b)

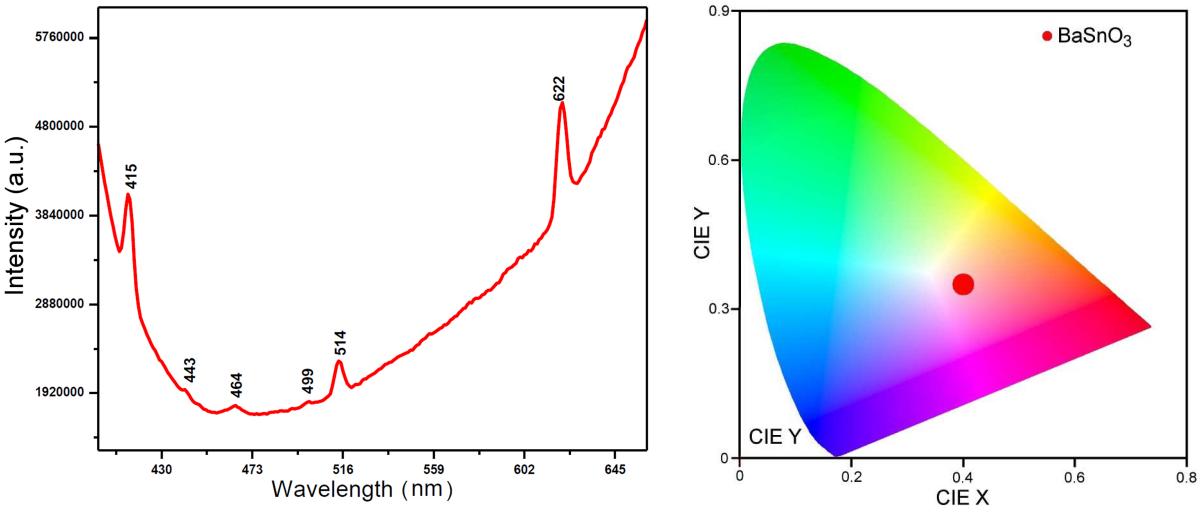

Figure 8. Photoluminescence (PL) spectra of $BaSnO_3$ powder calcined at 1400 °C (a) and CIE plot of photoluminescence spectrum of calcined powder (b)

Table 3. Wavelength corresponding to different transitions

No.	Wavelength [nm]	Barium (Ba)	Tin (Sn)
1	415	$^2P^0_{1/2}-^2D_{3/2}$	
2	443		$^1S_0-^1P^0_1$
3	464	$^2S_{1/2}-^2P^0_{3/2}$	
4	499	$^2S_{1/2}-^2P^0_{1/2}$	
5	514		$^2P^0_{1/2}-^2D_{3/2}$
6	622	$^3D_3-^3D^0_3$	

be attributed to the presence of defects in the material. The commission international del'Eclairage (CIE) coordinate has been calculated from the photoluminescence spectrum and indexed in CIE graph as shown in Fig. 8b. The CIE coordinate for $BaSnO_3$ obtained at 1400 °C is found to be $x = 0.40$, $y = 0.35$, which indicates that the emission has the contribution of red, blue and green (RBG). Therefore, the synthesized $BaSnO_3$ having emission in the visible region can find various applications in optical devices application like other phosphor materials [36].

IV. Conclusions

Thermal analysis of a stoichiometric mechanical mixture of $Ba(OH)_2$ and Na_2SnO_3 raw materials confirmed that no reaction between these starting materials takes place up to 1000 °C. However, when an aqueous solution of these starting materials was mixed and heated at 150 °C, amorphous phase of $BaSnO_3$ along with minor amounts of impurity phases $BaCO_3$ and SnO_2 occurred at 150 °C and crystallization of $BaSnO_3$ phase appeared at 800 °C. The phase pure $BaSnO_3$ powder was obtained after calcination at 1400 °C for 4 h. FTIR also confirmed that the $BaSnO_3$ powder obtained at 800 °C is contaminated with a trace amount of $BaCO_3$, whereas the powder obtained at 1400 °C is devoid of any impurity phase. TEM studies confirmed that the powder calcined at 1400 °C has cubical shape particles of ~25 nm in size, whereas XRD and Rietveld refinement showed that the powder has cubic structure with the lattice parameter $a = 4.1117(2)$ Å. The band gap determined from the UV-visible absorption spectrum of the phase pure $BaSnO_3$ powder is 3.09 eV which confirmed its semiconductor nature. PL spectra recorded in emission mode exhibited few intense peaks in the visible range. The corresponding CIE plot shows that the emission spectra of $BaSnO_3$ have the equal contributions of red, blue, and green which makes this material a promising candidate for the luminescence applications.

Acknowledgements: Authors are grateful to the Head of Department of Physics and the Head of Department of Pharmaceutics IIT(BUH), Varanasi for providing the experimental facilities required for this work. One of the authors Mr. Upendra Kumar is thankful to the Ministry of Human Resource and Development (MHRD), Government of India for providing financial support in terms of Senior Research Fellowship (SRF).

References

1. W. Zhang, J. Tang, J. Ye, "Structural, photocatalytic, and photophysical properties of perovskite $MSnO_3$ (M = Ca, Sr, and Ba) photocatalysts", *J. Mater. Res.*, **22** [7] (2007) 1859–1871.
2. S. Sallis, D.O. Scanlon, S.C. Chae, N.F. Quackenbush, D.A. Fischer, J.C. Woicik, J.-H. Guo, S.W. Cheong, L.F.J. Piper, "La-doped $BaSnO_3$ - degenerate perovskite transparent conducting oxide: Evidence from synchrotron X-ray spectroscopy", *Appl. Phys. Lett.*, **103** [4] (2013) 042105.
3. U.S. Alaan, P. Shafer, A.T. N'Diaye, E. Arenholz, Y. Suzuki, "Gd-doped $BaSnO_3$: A transparent conducting oxide with localized magnetic moments", *Appl. Phys. Lett.*, **108** [4] (2016) 042106.
4. H.J. Kim, U. Kim, T.H. Kim, J. Kim, H.M. Kim, B.-G. Jeon, W.-J. Lee, H.S. Mun, K.T. Hong, J. Yu, K. Char, K.H. Kim, "Physical properties of transparent perovskite

oxides (Ba,La)SnO_3 with high electrical mobility at room temperature", *Phys. Rev. B*, **86** [16] (2012) 165205.
5. S. Tao, F. Gao, X. Liu, O.T. Sørensen, "Ethanol-sensing characteristics of barium stannate prepared by chemical precipitation", *Sensors Actuators B: Chem.*, **71** [3] (2000) 223–227.
6. E. Sotter, X. Vilanova, E. Llobet, A. Vasiliev, X. Correi, "Thick film titania sensors for detecting traces of oxygen", *Sensors Actuators B: Chem.*, **127** [2] (2007) 567–579.
7. Y. Suzuki, Y. Okamoto, N. Ishii, "Dye-sensitized solar cells using double-oxide electrodes: A brief review", *J. Phys: Conference Series, IOP Publishing*, **596** [1] (2015) 012001.
8. N. Sharma, K.M. Shaju, G.V. Subba Rao, B.V.R. Chowdari, "Anodic behavior and X-ray photoelectron spectroscopy of ternary tin oxides", *J. Power Sources*, **139** [1-2] (2005) 250–260.
9. L. Li, J.C. Nino, "Proton-conducting barium stannates: doping strategies and transport properties", *Int. J. Hydrogen Energy*, **38** [3] (2013) 1598–1606.
10. Y. Wang, T. Su, W. Liu, Q. Chang, G. Qiao, "Effect of indium content on the properties of $BaSn_{0.5}Y_{0.5-x}In_xO_{2.75}$ proton conductor", *Ceram. Int.*, **41** [5B] (2015) 6863–6868.
11. S. Upadhyay, "High-temperature impedance spectroscopy of barium stannate, $BaSnO_3$", *Bull. Mater. Sci.*, **36** [6] (2013) 1019–1036.
12. J. Cerdà, J. Arbiol, R. Diaz, G. Dezanneau, J.R. Morante, "Synthesis of perovskite-type $BaSnO_3$ particles obtained by a new simple wet chemical route based on a sol-gel process", *Mater. Lett.*, **56** [3] (2002) 131–136.
13. A. Stanulis, S. Sakirzanovas, M. Van Bael, A. Kareiva, "Sol-gel (combustion) synthesis and characterization of different alkaline earth metal (Ca, Sr, Ba) stannates", *J. Sol-Gel Sci. Technol.*, **64** [3] (2012) 643–652.
14. W. Lu, H. Schmidt, "Preparation and characterization of $BaSnO_3$ powders by hydrothermal synthesis from tin oxide hydrate gel", *J. Mater. Sci.*, **42** [24] (2007) 10007–10013.
15. C. Huang, X. Wang, Q. Shi, X. Liu, Y. Zhang, F. Huang, T. Zhang, "A facile peroxo-precursor synthesis method and structure evolution of large specific surface area mesoporous $BaSnO_3$", *Inorg. Chem.*, **54** [8] (2015) 4002–4010.
16. W. Lu, H. Schmidt, "Lyothermal synthesis of nanocrystalline $BaSnO_3$ powders", *Ceram. Int.*, **34** [3] (2008) 645–649.
17. Y.H.O. Muñoz, M. Ponce, J. Enrique Rodríguez Páez, "Comparative study of two wet chemical methods of $BaSnO_3$ synthesis: mechanism of formation of mixed oxide", *Powder Technol.*, **279** (2015) 86–95.
18. C.P. Udawatte, M. Kakihana, M. Yoshimura, "Preparation of pure perovskite-type $BaSnO_3$ powders by the polymerized complex method at reduced temperature", *Solid State Ionics*, **108** [1] (1998) 23–30.
19. J. Ahmed, C.K. Blakely, S.R. Bruno, V.V. Poltavets, "Synthesis of $MSnO_3$ (M = Ba, Sr) nanoparticles by reverse micelle method and particle size distribution analysis by whole powder pattern modeling", *Mater. Res. Bull.*, **47** [9] (2012) 2282–2287.
20. S.S. Shukla, *Synthesis and dispersion of barium stannate nanopowders*, B.Sc. Thesis, Department of Ceramic Engineering, National Institute of Technology, Rourkela, India, 2011.
21. C. Huang, X. Wang, X. Liu, M. Tian, T. Zhang, "Extensive analysis of the formation mechanism of $BaSnO_3$ by solid-state reaction between $BaCO_3$ and SnO_2", *J. Eur. Ceram. Soc.*, **36** [3] (2016) 583–592.
22. Y.-Y. Di, Z.-C. Tan, L.-X. Sun. "Low-temperature heat capacities and thermodynamic properties of octahydrated barium dihydroxide, $Ba(OH)_2 \cdot 8\,H_2O$", *Chinese J. Chem.*, **25** [5] (2007) 587–591.
23. H.Q. Qu, W.H. Wu, N. Li, J.Z. Xu, "Thermal analysis method for studying the effects of a series of stannates on flame retardancy of wood by thermogravimetry-mass spectrometry", *Adv. Mater. Res.*, **197-198** (2011) 1447–1451.
24. S. Upadhyay, O. Parkash, D. Kumar. "Preparation and characterization of barium stannate $BaSnO_3$", *J. Mater. Sci. Lett.*, **16** [16] (1997) 1330–1332.
25. U. Sujana Kumari, P. Suresh, A.V. Prasada Rao, "Solid-state metathetic synthesis of phase pure $BaSnO_3$ and $BaZrO_3$", *Int. Res. J. Pure Appl. Chem.*, **3** [4] (2013) 347–356.
26. P. Durán, D. Gutierrez, J. Tartaj, M.A. Bañares, C. Moure, "On the formation of an oxycarbonate intermediate phase in the synthesis of $BaTiO_3$ from (Ba,Ti)-polymeric organic precursors", *J. Eur. Ceram. Soc.*, **22** [6] (2002) 797–807.
27. A.S. Deepa, S. Vidya, P.C. Manu, S. Solomon, A. John, J.K. Thomas, "Structural and optical characterization of $BaSnO_3$ nanopowder synthesized through a novel combustion technique", *J. Alloys Compd.*, **509** [5] (2011) 1830–1835.
28. C.V. Gopal Reddy, S.V. Manorama, V.J. Rao, "Preparation and characterization of barium stannate: application as a liquefied petroleum gas sensor", *J. Mater. Sci.: Mater. Electron.*, **12** [2] (2001) 137–142.
29. R.O. Kagel, R.A. Nyquist, *Infrared Spectra of Inorganic Compounds*, Academic Press, San Diego, USA, 1971.
30. Md. J. Ansaree, S. Upadhyay. "Electrical characterization of porous La-doped $BaSnO_3$ using impedance spectroscopy", *Ionics*, **21** [10] (2015) 2825–2838.
31. H. Mizoguchi, H.W. Eng, P.M. Woodward. "Probing the electronic structures of ternary perovskite and pyrochlore oxides containing Sn^{4+} or Sb^{5+}", *Inorg. Chem.*, **43** [5] (2004) 1667–1680.
32. L.B. Duan, G.H. Rao, Y.C. Wang, J. Yu, T. Wang, "Magnetization and Raman scattering studies of (Co, Mn) codoped ZnO nanoparticles", *J. Appl. Phys.*, **104** [1] (2008) 013909.
33. R. Köferstein, F. Yakuphanoglu, "Semiconducting properties of Ge-doped $BaSnO_3$ ceramic", *J. Alloys Compd.*, **506** [2] (2010) 678–682.
34. J.E. Sansonetti, W.C. Martin, "Handbook of basic atomic spectroscopic data", *J. Phys. Chem. Ref. Data*, **34** [4] (2005) 1559–2259.
35. Q. Zhu, J.-G. Li, C. Zhi, X. Li, X. Sun, Y. Sakka, D. Golberg, Y. Bando, "Layered rare-earth hydroxides (LRHs) of $(Y_{1-x}Eu_x)_2(OH) \cdot 5\,NO_3 \cdot n\,H_2O$ (x = 0–1): Structural variations by Eu^{3+} doping, phase conversion to oxides, and the correlation of photoluminescence behaviors", *Chem. Mater.*, **22** [14] (2010) 4204–4213.
36. R.C. Ropp, *Luminescence and the Solid State*, Vol. 12, Elsevier, Amsterdam, The Netherlands, 1991.